Bistable scattering in graphene-coated dielectric nanowires: supplementary material

Rujiang Li[1,2], Huaping Wang[1,3*], Bin Zheng[1,2], Shahram Dehdashti[1,2], Erping Li[1] and Hongsheng Chen[1,2†]

[1] *State Key Laboratory of Modern Optical Instrumentation, College of Information Science and Electronic Engineering, Zhejiang University, Hangzhou 310027, China*

[2] *The Electromagnetics Academy of Zhejiang University, Zhejiang University, Hangzhou 310027, China and*

[3] *Institute of Marine Electronics Engineering, Zhejiang University, Hangzhou 310058, China*

This document provides supplementary information to "Bistable scattering in graphene-coated dielectric nanowires".

I. THE FIRST ORDER SCATTERING TERM

For the graphene-coated dielectric nanowire, if the radius of the dielectric nanowire is far smaller than the wavelength, the total scattering is dominated by the first order scattering term. In the linear case where $I_0 = 0$, we show the normalized scattering cross sections (NSCSs) for different parameters in Fig. 1.

The graphene-coated dielectric nanowire can exhibit cloaking [1] and superscattering [2] at different frequencies. As shown in Fig. 1(a), superscattering occurs at a low frequency due to the resonance of the localized surface plasmonic mode, while cloaking occurs at a high frequency. If the chemical potential of graphene is small, both the frequencies for superscattering and cloaking show red shifts. According to the formula for the linear surface conductivity of graphene, the dissipation loss increases when the frequency decreases. Thus both the NSCSs at the superscattering and cloaking frequencies decrease with the decreasing of the chemical potential. Note in Fig. 1(a), $\hbar\omega \ll \mu_c$ are fulfilled for all the parameters.

Optical bistability is based on the nonlinear response of graphene. In order to enhance the local field intensity along the graphene coating, the working frequency of bistable scattering should be near to the superscattering frequency. Figs. 1(b)-(c) show the dependences between the NSCS and the incident frequency, where $\mu_c = 0.20$ eV and $\mu_c = 0.50$

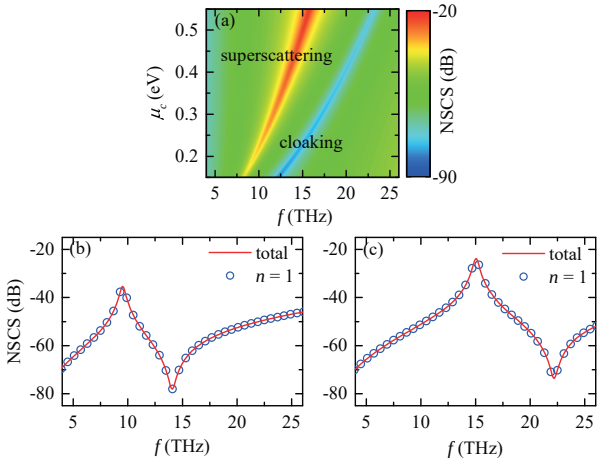

FIG. 1: (a) The normalized scattering cross sections (NSCSs) for different chemical potentials μ_c and at different frequencies f. (b)-(c) The dependences between the NSCS and the incident frequency, where $\mu_c = 0.20$ eV in (b) and $\mu_c = 0.50$ eV in (c). For comparison, the contributions from the $n = 1$ scattering terms are also plotted. The relaxation time of graphene is $\tau = 0.30$ ps. The relative permittivity and permeability of the dielectric nanowire are $\varepsilon_r = 2.7$ and $\mu_r = 1$, respectively, and the radius of the nanowire is $R = 200$ nm.

* hpwang@zju.edu.cn
† hansomchen@zju.edu.cn

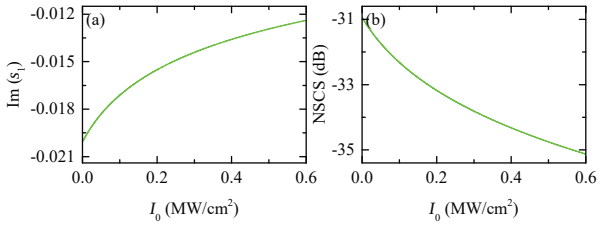

FIG. 2: (a) The scattering coefficients and (b) NSCSs for different incident field intensities, where $f = 13.00$ THz, $\mu_c = 0.35$ eV, and $\tau = \infty$.

eV, respectively. In Fig. 1(b), according to the formula for the nonlinear surface conductivity of graphene, the nonlinear surface conductivity is large due to the small chemical potential and low superscattering frequency, although the local field intensity is weak. While in Fig. 1(c), the nonlinear surface conductivity is small, but the local field intensity is large due to the enhanced NSCS. The nonlinear surface conductivity and the local field intensity are contradictory to each other. Besides, as shown in Figs. 1(b)-(c), the NSCSs are dominated by the $n = 1$ scattering term. This implies that it is enough to only consider the first order scattering coefficient s_1 in the study of bistable scattering.

II. NOTES ON NONLINEAR SCATTERING MODEL

Before using the approximations of $k_0 R \ll 1$ and $kR \ll 1$, from the two boundary conditions of E_θ and H_z, we obtain a cubic nonlinear equation for the first order scattering coefficient s_1:

$$c^{(1)} + c_1^{(1)} s_1 + c_{1^*}^{(1)} s_1^* + c_{11}^{(1)} s_1^2 + c_{11^*}^{(1)} |s_1|^2 + c_{11^*1}^{(1)} |s_1|^2 s_1 = 0. \tag{1}$$

In this equation, the coefficients for each term are

$$c^{(1)} = \gamma_{111}^{(1)} J_1'^3 (k_0 R) + \left[J_1' (k_0 R) t_1 - J_1 (k_0 R) J_1' (kR) \right], \tag{2}$$

$$c_1^{(1)} = 2\gamma_{111}^{(1)} J_1'^2 (k_0 R) H_1^{(1)\prime} (k_0 R) + \left[H_1^{(1)\prime} (k_0 R) t_1 - H_1^{(1)} (k_0 R) J_1' (kR) \right], \tag{3}$$

$$c_{1^*}^{(1)} = \gamma_{111}^{(1)} J_1'^2 (k_0 R) H_1^{(1)\prime *} (k_0 R), \tag{4}$$

$$c_{11}^{(1)} = \gamma_{111}^{(1)} J_1' (k_0 R) H_1^{(1)\prime 2} (k_0 R), \tag{5}$$

$$c_{11^*}^{(1)} = 2\gamma_{111}^{(1)} J_1' (k_0 R) \left| H_1^{(1)\prime} (k_0 R) \right|^2, \tag{6}$$

$$c_{11^*1}^{(1)} = \gamma_{111}^{(1)} \left| H_1^{(1)\prime} (k_0 R) \right|^2 H_1^{(1)\prime} (k_0 R), \tag{7}$$

the coefficient that is related with $\sigma_g^{(3)}$ is $\gamma_{111}^{(1)} = \alpha \varepsilon_r |a_1|^2 J_1' (kR)$, and $t_1 = \sqrt{\varepsilon_r} J_1 (kR) + i\sigma_g^{(1)} \eta_0 J_1' (kR)$. Specially, if the nonlinear surface conductivity of graphene is neglected, namely in the limit of $H_0 = 0$, the scattering coefficient reduces to

$$s_1 = -\frac{J_1' (k_0 R) t_1 - J_1 (k_0 R) J_1' (kR)}{H_1^{(1)\prime} (k_0 R) t_1 - H_1^{(1)} (k_0 R) J_1' (kR)}. \tag{8}$$

III. NOTES ON BISTABLE SCATTERING

A. Lossless case

If the working frequency is larger than the superscattering frequency, there is only one real solution and no bistable scattering occurs. Figs. 2(a)-(b) show the scattering coefficients and NSCSs for different incident field intensities at $f = 13.00$ THz. If the incident field intensity is large enough, the first term in the discriminant of the cubic nonlinear

equation can be neglected and the scattering coefficient reduces to

$$\operatorname{Im} s_1 = \frac{\pi k_0^2 R^2}{2} \sqrt[3]{\frac{k_0 R}{\sigma_{g,i}^{(3)} \eta_0^2 I_0}} + \frac{\pi k_0^2 R^2}{4}. \tag{9}$$

As shown in Figs. 2(a)-(b), with the increasing of the incident field intensity, the scattering coefficient increases but the NSCS decreases.

B. Lossy case

In the lossy case, the nonlinear equation reduces to

$$c^{(1)} + c_1^{(1)} s_1 + c_{1^*}^{(1)} s_1^* + c_{11}^{(1)} s_1^2 + c_{11^*}^{(1)} |s_1|^2 + c_{11^*1}^{(1)} |s_1|^2 s_1 = 0, \tag{10}$$

where the coefficient are

$$c^{(1)} = \frac{i\sigma_g^{(3)} \eta_0^2 I_0}{8} + \frac{1}{2}\left[(\varepsilon_r - 1) k_0 R + i\sigma_g^{(1)} \eta_0\right], \tag{11}$$

$$c_1^{(1)} = -\frac{\sigma_g^{(3)} \eta_0^2 I_0}{\pi k_0^2 R^2} + i\frac{2}{\pi k_0^2 R^2}\left[(\varepsilon_r + 1) k_0 R + i\sigma_g^{(1)} \eta_0\right], \tag{12}$$

$$c_{1^*}^{(1)} = \frac{\sigma_g^{(3)} \eta_0^2 I_0}{2\pi k_0^2 R^2}, \tag{13}$$

$$c_{11}^{(1)} = -\frac{2i\sigma_g^{(3)} \eta_0^2 I_0}{\pi^2 k_0^4 R^4}, \tag{14}$$

$$c_{11^*}^{(1)} = \frac{4i\sigma_g^{(3)} \eta_0^2 I_0}{\pi^2 k_0^4 R^4}, \tag{15}$$

$$c_{11^*1}^{(1)} = -\frac{8\sigma_g^{(3)} \eta_0^2 I_0}{\pi^3 k_0^6 R^6}, \tag{16}$$

and $I_0 = \eta_0 H_0^2/2$ is the incident field intensity. Specially, when $I_0 = 0$,

$$s_1 = i\frac{\pi k_0^2 R^2}{4} \frac{(\varepsilon_r - 1) k_0 R + i\sigma_g^{(1)} \eta_0}{(\varepsilon_r + 1) k_0 R + i\sigma_g^{(1)} \eta_0}. \tag{17}$$

To further simplify the equation, we can separate the real and imaginary parts, where $s_1 = s_{1r} + i s_{1i}$. The equation simplifies to

$$c_r^{(1)} + c_{1r}^{(1)} s_{1r} - \left(c_{1i}^{(1)} - c_{1^*i}^{(1)}\right) s_{1i} + \left(c_{11r}^{(1)} + c_{11^*r}^{(1)}\right) s_{1r}^2 - \left(c_{11r}^{(1)} - c_{11^*r}^{(1)}\right) s_{1i}^2 - c_{11^*1i}^{(1)} s_{1r}^2 s_{1i} - c_{11^*1i}^{(1)} s_{1i}^3 = 0, \tag{18}$$

$$c_i^{(1)} + \left(c_{1i}^{(1)} + c_{1^*i}^{(1)}\right) s_{1r} + c_{1r}^{(1)} s_{1i} + 2c_{11r}^{(1)} s_{1r} s_{1i} + c_{11^*1i}^{(1)} s_{1r}^3 + c_{11^*1i}^{(1)} s_{1r} s_{1i}^2 = 0, \tag{19}$$

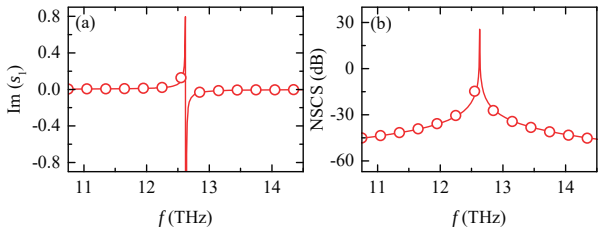

FIG. 3: (a) The scattering coefficients and (b) NSCSs at different frequencies, where $I_0 = 0$, $\mu_c = 0.35$ eV, and $\tau = \infty$. The sold curve is obtained from the nonlinear scattering model with approximations of $k_0 R \ll 1$ and $kR \ll 1$, and the scatter diagram is obtained without approximations.

where

$$c_r^{(1)} = -\frac{\sigma_{g,i}^{(3)} \eta_0^2 P_0}{8} + \frac{1}{2}\left[(\varepsilon_r - 1)\, k_0 R - \sigma_{g,i}^{(1)} \eta_0\right], \tag{20}$$

$$c_i^{(1)} = \frac{\sigma_{g,r}^{(1)} \eta_0}{2}, \tag{21}$$

$$c_{1,r}^{(1)} = -\frac{2\sigma_{g,r}^{(1)} \eta_0}{\pi k_0^2 R^2}, \tag{22}$$

$$c_{1,i}^{(1)} = -\frac{\sigma_{g,i}^{(3)} \eta_0^2 P_0}{\pi k_0^2 R^2} + \frac{2}{\pi k_0^2 R^2}\left[(\varepsilon_r + 1)\, k_0 R - \sigma_{g,i}^{(1)} \eta_0\right], \tag{23}$$

$$c_{1^*,i}^{(1)} = \frac{\sigma_{g,i}^{(3)} \eta_0^2 P_0}{2\pi k_0^2 R^2}, \tag{24}$$

$$c_{11,r}^{(1)} = \frac{2\sigma_{g,i}^{(3)} \eta_0^2 P_0}{\pi^2 k_0^4 R^4}, \tag{25}$$

$$c_{11^*,r}^{(1)} = -\frac{4\sigma_{g,i}^{(3)} \eta_0^2 P_0}{\pi^2 k_0^4 R^4}, \tag{26}$$

$$c_{11^*1,i}^{(1)} = -\frac{8\sigma_{g,i}^{(3)} \eta_0^2 P_0}{\pi^3 k_0^6 R^6}. \tag{27}$$

This coupled nonlinear equation can be solved numerically.

IV. BISTABLE SCATTERING WITHOUT APPROXIMATIONS

In the nonlinear scattering model, we use the approximations of $k_0 R \ll 1$ and $kR \ll 1$, and the Bessel function and Hankel function are replaced by their respective asymptotic expansions, respectively. We will discuss in the following that this kind of approximation is acceptable.

A. Lossless case

First we consider a special case. Fig. 3 shows the comparison between the scatterings in the linear case with and without approximations, where $I_0 = 0$ and $\tau = \infty$. In the nonlinear scattering model, when we take the approximations of $k_0 R \ll 1$ and $kR \ll 1$, the real part of the Hankel function is neglected, which leads to the breaking of the single channel limit [3]. At the superscattering frequency, the NSCS is infinite in the approximate model, but it equals to a finite value (3.01 dB in this structure) when there are no approximations. However, this kind of approximation is acceptable since the working frequency of bistable scattering is near but not very close to the superscattering frequency. For example, at $f = 12.00$ THz, the solid curve agrees well with the scatter diagram.

In the nonlinear case, we consider the scatterings at $f = 13.00$ THz and $f = 12.00$ THz, respectively. As shown in Fig. 4, there is no bistable scattering at $f = 13.00$ THz, where the solid curves are calculated from the nonlinear

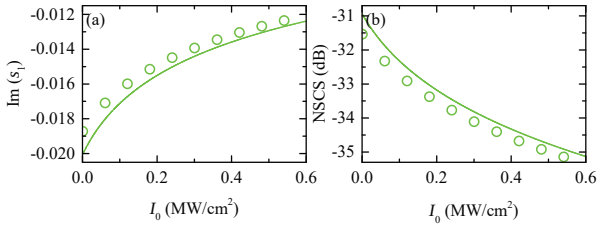

FIG. 4: (a) The scattering coefficients and (b) NSCSs for different incident field intensities, where $f = 13.00$ THz, $\mu_c = 0.35$ eV, and $\tau = \infty$. The solid curves are calculated from the nonlinear scattering model with approximations of $k_0R \ll 1$ and $kR \ll 1$, which are the same with that in Fig. 2. The scatter diagrams are calculated without approximations.

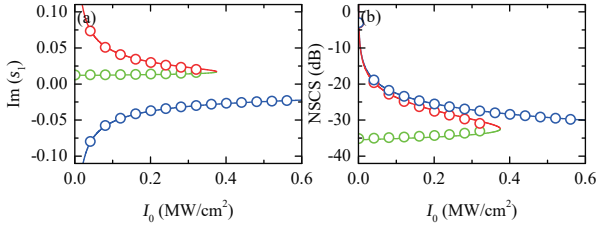

FIG. 5: (a) The scattering coefficients and (b) NSCSs for different incident field intensities, where $f = 12.00$ THz, $\mu_c = 0.35$ eV, and $\tau = \infty$. The solid curves are calculated from the nonlinear scattering model with approximations of $k_0R \ll 1$ and $kR \ll 1$, and the scatter diagrams are calculated without approximations. The curves or scatter diagrams with different colors corresponds to different branches.

scattering model with approximations of $k_0R \ll 1$ and $kR \ll 1$, and the scatter diagrams are calculated without approximations. The scatter diagrams deviate a little from the solid curves when the incident filed intensity is small, since the working frequency is a little near to the superscattering frequency. However, their scattering behaviors are totally the same and there are no bistable scatterings in the scattering models with and without approximations.

At $f = 12.00$ THz, bistable scattering occurs as shown in Fig. 5. The solid curves calculated with approximations agree well with the scatter diagrams calculated without approximations. The only difference is the switching-up intensity. For the model without approximations, T_{on} is decreased slightly. But this difference is not obvious to affect the bistable scattering.

B. Lossy case

In the lossy case, the solid curves calculated with approximations of $k_0R \ll 1$ and $kR \ll 1$ also agree well with the scatter diagrams calculated without approximations, as shown in Fig.6. Compared with the bistable scattering shown by the solid curves, the bistable scattering shown by the scatter diagrams have smaller switching-up and

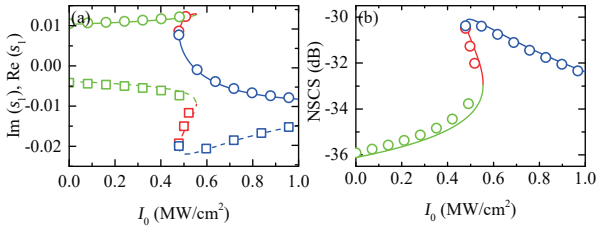

FIG. 6: (a) The scattering coefficients and (b) NSCSs for different incident field intensities, where $f = 12.00$ THz, $\mu_c = 0.35$ eV, and $\tau = 0.30$ ps. The solid curves are calculated from the nonlinear scattering model with approximations of $k_0R \ll 1$ and $kR \ll 1$, and the scatter diagrams are calculated without approximations. In (a), the solid curve and circles denote Im (s_1), and the dashed curve and squares denote Re (s_1). The curves or scatter diagrams with different colors corresponds to different branches.

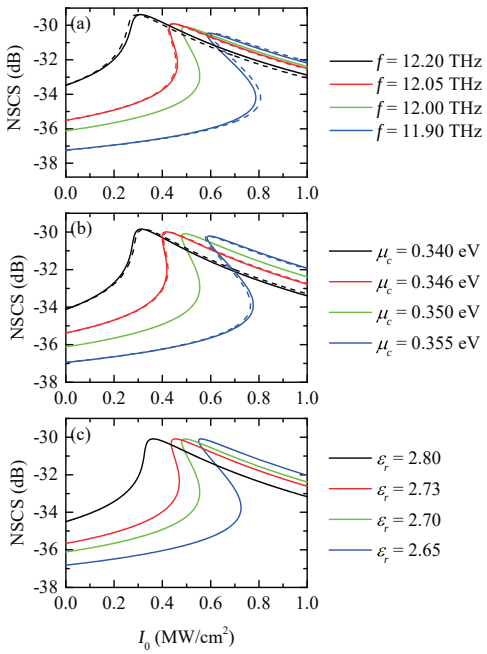

FIG. 7: (a) The NSCSs for different working frequencies, where $\mu_c = 0.350$ eV, $\tau = 0.30$ ps, and the values of f are taken as 11.90 THz (blue curve), 12.00 THz (green curve), 12.05 THz (red curve), and 12.20 THz (black curve), respectively. For comparison, the dashed curves for a fixed nonlinear surface conductivity where $f = 12.00$ THz are also plotted. (b) The NSCS for different chemical potentials of graphene, where $f = 12.00$ THz, $\tau = 0.30$ ps, and the values of μ_c are taken as 0.355 eV (blue curve), 0.350 eV (green curve), 0.346 eV (red curve), and 0.340 eV (black curve), respectively. For comparison, the dashed curves for a fixed nonlinear surface conductivity where $\mu_c = 0.350$ eV are also plotted. (c) The NSCS for different permittivities of the dielectric nanowire, where $f = 12.00$ THz, $\mu_c = 0.350$ eV, $\tau = 0.30$ ps, and the values of ε_r are taken as 2.65 (blue curve), 2.70 (green curve), 2.73 (red curve), and 2.80 (black curve), respectively.

switching-down intensities. But this change is very small and it is acceptable for the study of bistable scattering.

V. NOTES ON DISCUSSION

In the main manuscript, we have discussed the bistable scatterings at different working frequencies. According to the nonlinear surface conductivity of graphene, the shift of the working frequency also induces a change of the nonlinear surface conductivity. However, this change has a weak contribution to the NSCS. In Fig. 7(a), for a fixed working frequency, there are two curves: one solid curve and one dashed curve. For the solid curve, both the linear and nonlinear surface conductivities are calculated at the given working frequency. While for the dashed curve, the linear surface conductivity is calculated at the given working frequency, but the nonlinear surface conductivity is calculated at a fixed frequency $f = 12.00$ THz. By comparing the solid and dashed curves, we know that the change of the nonlinear surface conductivity induced by the shift of the working frequency has a weak contribution to the bistable scattering.

The chemical potential of graphene also plays an important role to determine the bistable scattering. According to Ref. [2], the superscattering frequency depends on the chemical potential. If the chemical potential increases, the superscattering frequency also increases. In the bistable scattering, the blue shift of the superscattering frequency is equivalent with the red shift of the working frequency. To validate this prediction, we show the NSCSs for different chemical potentials of graphene in Fig. 7(b), where $f = 12.00$ THz, $\tau = 0.30$ ps, and $\varepsilon_r = 2.7$.

As shown by the solid blue curve in Fig. 7(b), if the chemical potential increases, the corresponding superscattering frequency increases and the equivalent working frequency decreases. Thus the switching threshold is increased. However, if the chemical potential of graphene decreases, the corresponding superscattering frequency decreases and the equivalent working frequency increases. Thus the switching threshold is decreased, as shown by the solid red curve. If the chemical potential continues to decrease, the switching threshold decreases and the bistable scattering disappears gradually.

According to the nonlinear surface conductivity of graphene, the nonlinear surface conductivity depends on the chemical potential. However, the shift of the NSCS is mainly due to the shift of the superscattering frequency. The contribution from the change of the nonlinear surface conductivity is small. For comparison, in Fig. 7(b), we also plot the NSCSs for a fixed nonlinear surface conductivity where $\mu_c = 0.350$ eV. The change of the nonlinear surface conductivity only adds a perturbation to the shift of the NSCS.

The permittivity of the dielectric nanowire is also an important parameter to determine the bistable scattering. According to Ref. [2], the superscattering frequency depends on the permittivity of the dielectric nanowire. If the permittivity increases, the superscattering frequency decreases. In the bistable scattering, the red shift of the superscattering frequency is equivalent with the blue shift of the working frequency. To validate this prediction, we show the NSCSs for different permittivities of the dielectric nanowire in Fig. 7(c), where $f = 12.00$ THz, $\mu_c = 0.350$ eV, and $\tau = 0.30$ ps.

As shown by the solid blue curve, if the permittivity decreases, the superscattering frequency increases and the working frequency decreases. Thus the switching threshold is increased. Whereas, if the permittivity increases, the switching threshold is decreased, as shown by the solid red curve. If the permittivity continues to increase, the bistable scattering disappears gradually, as shown by the solid black curve.

[1] P.-Y. Chen, and A. Alù, *Atomically Thin Surface Cloak Using Graphene Monolayers*, ACS Nano, **5**, 5855 (2011).
[2] R. Li, X. Lin, S. Lin, X. Liu, and H. Chen, *Tunable deep-subwavelength superscattering using graphene monolayers*, Opt. Lett. **40**, 1651 (2015).
[3] Z. Ruan and S. Fan, *Superscattering of Light from Subwavelength Nanostructures*, Phys. Rev. Lett. **105**, 013901 (2010).